Acute loss of adipose tissue-derived adiponectin triggers immediate metabolic deterioration in mice

Jonathan Y. Xia[1,2], **Kai Sun**[1,3], **Chelsea Hepler**[1], **Alexandra L. Ghaben**[1], **Rana K. Gupta**[1], **Yu A. An**[1], **William L. Holland**[1], **Thomas S. Morley**[1], **Andrew C. Adams**[4], **Ruth Gordillo**[1], **Christine M. Kusminski**[1], and **Philipp E. Scherer**[1,5]

[1]Touchstone Diabetes Center, Department of Internal Medicine, The University of Texas Southwestern Medical Center, 5323 Harry Hines Blvd, MC8549, Dallas, TX 75390-8549, USA

[2]McGaw Medical Center of Northwestern University, Department of Internal Medicine, Chicago, IL, USA

[3]Center for Metabolic and Degenerative Diseases, Institute of Molecular Medicine, University of Texas Health Science Center at Houston. Houston, TX, USA

[4]Lilly Research Laboratories, Division of Eli Lilly and Company, Indianapolis, IN, USA

[5]Department of Cell Biology, The University of Texas Southwestern Medical Center, Dallas, Texas, USA

Abstract

Aim/hypothesis—Adiponectin (APN), a circulating hormone secreted by mature adipocytes, has been extensively studied because it has beneficial metabolic effects. While many studies have focused on the congenital loss of APN and its effects on systemic body glucose and lipid metabolism, little is known about the effects triggered by acute loss of APN in the adult mouse. We anticipated that genetically induced acute depletion of APN in adult mice would have a more profound effect on systemic metabolic health than congenital deletion of *Adipoq*, the gene encoding APN, with its associated potential for adaptive responses that may mask the phenotypes.

Methods—Mice carrying loxP-flanked regions of *Adipoq* were generated and bred to the *Adipoq* (APN) promoter-driven reverse tetracycline-controlled transactivator (rtTA) (APN-rtTA) gene and a *tet*-responsive Cre line (TRE-Cre) to achieve acute depletion of APN. Upon acute removal of APN in adult mice, systemic glucose and lipid homeostasis were assessed under basal and insulinopenic conditions.

Results—The acute depletion of APN results in more severe systemic insulin resistance and hyperlipidaemia than in mice with congenital loss of APN. Furthermore, the acute depletion of APN in adult mice results in a much more dramatic reduction in survival rate, with 50% of inducible knockouts dying in the first 5 days under insulinopenic conditions compared with 0% of congenital *Adipoq* knockout mice under similar conditions.

Conclusions/interpretation—Acute systemic removal of APN results in a much more negative metabolic phenotype compared with congenital knockout of *Adipoq*. Specifically, our data demonstrate that acute depletion of APN is especially detrimental to lipid homeostasis, both under basal and insulinopenic conditions. This suggests that compensatory mechanisms exist in congenital knockout mice that offset some of the metabolic actions covered by APN.

Introduction

Since its discovery in the mid-1990s, adiponectin (APN), an adipocyte-derived secretory protein, has been widely studied given its insulin sensitising, anti-inflammatory, proangiogenic and antiapoptotic effects on a number of different cell types [1]. Circulating and local APN exerts many important functions [2]. However, unlike the majority of adipokines, the expression levels for APN are inversely correlated with adipose tissue expansion and obesity [3]. In addition, circulating APN promotes insulin sensitivity by acting on peripheral tissues, such as the liver, adipose tissue and muscle, to decrease gluconeogenesis and enhance glucose uptake [4, 5].

Although profound beneficial metabolic effects of gain-of-function *Adipoq* (encoding APN) models have been demonstrated through both the   gly model and, more recently, overexpression of APN receptors [6, 7], loss-of-function models of *Adipoq* have had varying outcomes regarding metabolic phenotype. Studies by Kubota et al and Maeda et al showed mild-to-moderate insulin resistance and glucose intolerance in APN-deficient mice [8, 9]. However, Ma et al described no effects of knocking out *Adipoq* on systemic insulin sensitivity, but showed an unexpected increase in fatty acid oxidation in skeletal muscle [10]. The diversity in metabolic phenotypes of these congenital *Adipoq* (APN) null (APNKO) mice may be attributed to environmental or genetic factors. Furthermore, the methods for gene targeting and disruption varied in these models. The unique phenotype in the model by Ma and colleagues is probably due to a unique approach towards gene disruption that results in a gain rather than a loss of function. Interestingly, the APNKO model constructed by our group in 2005, which deleted all three exons and the 5′-untranslated region, displayed severe hepatic and, to a lesser degree, peripheral insulin resistance in muscle [11]. Although these constitutive APNKO models exhibit mild-to-moderate levels of insulin resistance and glucose intolerance, the negative effects on metabolic health are less severe than would be predicted based on the many roles attributed to APN.

The phenotypic variance of the congenital APNKO models may also be partially attributed to compensatory mechanisms during development. To overcome this and to further

investigate the physiological effects of an acute depletion of APN in adult mice, we have developed a mouse carrying a floxed *Adipoq* locus, which allows us to acutely delete *Adipoq* under the control of *tet*-responsive Cre (TRE-Cre). Using the *Adipoq* (APN) promoter-driven reverse tetracycline-controlled transactivator (APN-rtTA), we target *Adipoq* deletion in mature adipocytes upon doxycycline treatment. The availability of a mouse carrying loxP-flanked regions of the *Adipoq* gene enables us, for the first time, to probe the impact of a genetically induced acute depletion of APN on systemic metabolic health in the adult mouse.

Methods

Animals and diets

The work described in this manuscript has been approved and conducted under the oversight of the University of Texas Southwestern (UTSW) Institutional Animal Care and Use Committee. The APN-rtTA and TRE-Cre mice (JAX 006234; Jackson Laboratories, Bar Harbor, ME, USA) have been described previously [12]. The generation of *Adipoq* floxed (APN$^{fl/fl}$) mice is described in the electronic supplementary material (ESM) Methods: Generation of floxed adiponectin locus. All mice were maintained on a C57BL/6 background and experiments were conducted using male littermates as controls. APN-rtTA mice were bred with TRE-Cre mice and APN$^{fl/fl}$ mice to achieve doxycycline-inducible deletion of APN in mature adipocytes of adult mice (hereafter, inducible knockout [iKO] mice). Mice were housed in a barrier-free facility on a 12 h light/dark cycle in a temperature-controlled environment with free access to food and water. Mice were fed a standard chow with doxycycline (chow-dox; Bio-Serv S4107) or a high-fat diet with doxycycline (HFD-dox; 60% energy from fat; Bio-Serv S5867) (600 mg/kg doxycycline; Bio-Serv, Flemington, NJ, USA), or a high-fat diet (HFD; 60% energy from fat; Research Diets D12492, New Brunswick, NJ, USA) containing pioglitazone (40 mg/kg add-mix).

Tissue and serum immunoblotting

For tissue immunoblotting, frozen tissues were homogenised in RIPA buffer containing a protease inhibitor cocktail (Sigma P8340, St Louis, MO, USA). The homogenates were centrifuged and supernatant fractions were assayed for protein using a BCA assay (Thermo Fisher Scientific 23225, Waltham, MA, USA). Tissue protein (20 μg) or serum (0.1 μl) was separated by SDS-PAGE, transferred to nitrocellulose membranes and blotted with anti-mouse APN monoclonal antibodies (1:1000; produced in-house) [13]. The APN antibody was validated using serum from APNKO (negative control) and wild-type (WT) mice (positive control). Primary antibodies were detected using secondary antibodies labelled with infrared dyes emitting at 700 nm or 800 nm (1:5000; Li-Cor Bioscience 926-32220 and 926-32211, respectively), and visualised on a Li-Cor Odyssey infrared scanner (Li-Cor Bioscience, Lincoln, NE, USA). The scanned data were analysed and quantified using Odyssey version 2.1 software (Li-Cor Bioscience). Please refer to ESM Methods: Tissue and rerum immunoblotting, for additional information.

Body fat quantification

Total body lean mass and fat were quantified using a Bruker MQ10 NMR analyser (Bruker, Billerica, MA, USA).

Lipid quantifications

Sphingolipids were quantified by liquid chromatography–electrospray ionisation–tandem mass spectrometry using a Nexera UHPLC coupled to an LCMS-8050 (Shimadzu Scientific Instruments, Columbia, MD, USA) as described previously [14]. Data were processed using the LabSolutions V 5.82 and LabSolutions Insight V 2.0 program packages (Shimadzu Scientific Instruments).

Diacylglycerol and C17 NEFA were quantified using an ABI 5600+ (AB Sciex, Framingham, MA, USA); data were calibrated with Analyst V 1.6.3 (https://sciex.com/products/software/analyst-software) and PeakView V 2.0 (https://sciex.com/products/software/peakview-software) software (AB Sciex) [14]. Lipid species were identified based on exact mass and fragmentation patterns, and verified by lipid standards.

Systemic tests—For OGTTs and insulin tolerance tests, mice were fasted for 3 h prior to administration of glucose (2.5 g/kg bodyweight by gastric gavage; Sigma) or insulin (0.75 U/kg Humulin R; Eli Lilly, Indianapolis, IN, USA). For triacylglycerol tolerance tests (TGTTs), mice were fasted overnight, then orally gavaged with 20% intralipid (15 μl/g; Sigma I141). In the hepatic VLDL-triacylglycerol production assay, mice fasted for 5 h received an intravenous injection of 10% tyloxapol (500 mg/kg; Sigma T8761). Tail venous blood samples were collected. Glucose, insulin and triacylglyceride levels were measured using an oxidase-peroxidase assay (Sigma P7119), insulin ELISA (Millipore EZRMI-13K, Billerica, MA, USA) and Infinity Triglycerides Reagent (Thermo Fisher Scientific TR22421). Measurements of endogenous triolein clearance rates, tissue-specific lipid uptake and β-oxidation rates in transgenic tissues were performed as previously described [15]. Please refer to ESM Methods: ^{3}H-triolein uptake and β-oxidation, for in depth detail of lipid studies.

Hyperinsulinaemic–euglycaemic clamps

Hyperinsulinaemic–euglycaemic clamps were performed on conscious, unrestrained male mice as previously described [15].

Mitochondrial assay

Hepatic oxygen consumption rates (OCRs) were determined using the XF24 Extracellular Flux Analyzer (Seahorse Bioscience, North Billerica, MA, USA) as previously described [15].

STZ administration and FGF21 stimulation of adipocytes

Following a 6 h fast, mice were received a single intraperitoneal injection of streptozotocin (STZ; 200 μg/g; Sigma S1030). Following a 4 h fast, mice were intraperitoneally injected with fibroblast growth factor 21 (FGF21; 2 mg/kg; Eli Lilly LY240,5319).

Gene expression analysis

RNA was isolated following tissue homogenisation in Trizol (Invitrogen, Carlsbad, CA, USA) using a TissueLyser (Roche; Indianapolis, IN, USA) and RNeasy RNA extraction kit (Qiagen 74104, Germantown, MD, USA). cDNA was prepared using iScript cDNA Synthesis Kit (Bio-Rad 1708891, Hercules, CA, USA). qPCR was performed using SYBR Select Master Mix (Thermo Fisher 4472908). mRNA levels of *Rps18*, *Adipoq*, *Adipsin* (also known as *Cfd*), *Cebpa*, *Fabp4*, *Lpl*, *PPARγ2* (*Pparg*), *Lck*, *Lsp1*, *Col1a1* (*Col1a1*), *Col3a1* (*Col3a1*), *Cd6*, *Cd27*, *Cd52*, *Cd79A* and *Ccl19* were analysed using qPCR (see ESM Table 1 for a list of primers). mRNA levels were calculated using the Ct method [16], with *Rps18* used for normalisation.

Following HFD feeding for 4 weeks, iKO (*n*=3) and WT (*n*=3) mice received HFD-dox for 2 weeks, resulting in complete depletion of serum APN. Tissues were collected 3 days later. Global gene expression profiling was conducted on subcutaneous white adipose tissue (sWAT) and liver samples by the UTSW Genomics and Microarray Core (Dallas, TX, USA). Gene ontology analyses were performed using the DAVID Functional Annotation Tool (https://david.ncifcrf.gov/) and a primary component analysis was performed using RStudio v3.3 (https://www.rstudio.com/products/rstudio/download/); the heatmap was generated using the Pheatmap package (https://cran.r-project.org/web/packages/pheatmap/pheatmap.pdf).

Computed tomography

A computed tomography (CT) scan was performed on anaesthetised mice (eXplore Locus in vivo MicroCT; GE Healthcare, Buckingham, UK) as previously described [17].

Immunohistochemistry

Paraffin-embedded sections were incubated with anti-F4/80 (1:500; Bio-Rad MCA497), followed by biotinylated anti-rat secondary antibody (1:200; Vector BA-9400, Burlingame, CA, USA), horseradish peroxidase-conjugated streptavidin (1:200; Dako P0307, Santa Clara, CA, USA) and 3,3′-diaminobenzidine substrate (Thermo Fisher Scientific 34002).

In situ hybridisation

RNAscope 2.5 HD Assay-Brown (Bio-Techne, Minneapolis, MN, USA) was used for detecting *Adipoq* RNA in adipose tissue [18]. Please refer to ESM Methods: In situ hybridisation, for in depth detail on this.

LPL activity assay

Lipase activity was measured as previously described [19] with minor modifications. Briefly, plasma was collected before and 15 min after tail vein injection of heparin (1.5 U/g; Sigma H3393). Plasma was incubated with a triacylglycerol (TG) emulsion containing ~10^7 cpm/ml ^{3}H-triolein (PerkinElmer NET431001MC; Waltham, MA, USA) for total lipase activity or 1.5 mol/l NaCl for hepatic lipase activity. After centrifugation, the NEFA-containing aqueous phase was assayed for ^{3}H radioactivity on a scintillation counter. Plasma lipoprotein lipase (LPL) activity was calculated by subtracting the hepatic from the total

lipase activity. Please refer to ESM section lipoprotein lipase activity assay for in depth detail of this.

Statistics

All results are provided as means ± SEM. All statistical analyses were performed using GraphPad Prism version 7.0 (www.graphpad.com/scientific-software/prism/). Differences between the two groups over time were determined by a two-way repeated measures ANOVA. For comparisons between two independent groups, a Student's *t* test was used. Significance was accepted at $p < 0.05$. No experimental data was excluded and all experiments reflect a minimum of two independent experiments with separate littermate-controlled cohorts (see ESM Table 2).

Results

Generation of iKO mice

To investigate the acute effects of APN depletion, we generated a mouse model harbouring a loxP modified *Adipoq* allele. Specifically, the first two exons of the *Adipoq* gene were flanked by loxP sites (ESM Fig. 1a). A 230 bp product was amplified for the WT allele using specific genotyping primers that run through the region upstream of exon 1 of *Adipoq*. A PCR product of 330 bp was obtained for the region upstream of exon 1 of *Adipoq*, which includes the loxP site for the floxed *Adipoq* allele. Heterozygous mice were identified by the presence of both bands when the PCR product was analysed on a 1% agarose gel (ESM Fig. 1b). The iKO mouse was generated by breeding APN$^{fl/fl}$ mice with mice harbouring the APN-rtTA and TRE-Cre transgenes (ESM Fig. 1c). iKO mice fed chow-dox have undetectable serum APN within 14 days, while mice lacking either the APN-rtTA or TRE-Cre transgenes have similar levels of serum APN as iKO mice not fed doxycycline (ESM Fig. 1d).

Inducible elimination of APN increases hepatic ceramide levels and induces insulin resistance

We previously noted that APN confers ceramidase activity through its receptors [14] and, thus, tissue ceramide levels are a functional readout of APN action. To test the effects of acute depletion of APN on liver and adipose tissue ceramide levels, we initially challenged iKO and WT mice with an HFD for 6 weeks. Acute APN depletion was then induced with HFD-dox for 2 weeks. We verified that in iKO mice circulating APN is markedly reduced within 3 days of doxycycline treatment after HFD feeding (Fig. 1a). Low levels of APN are detectable up to 10 days after doxycycline exposure and become undetectable within 14 days.

Furthermore, the iKO mice showed a significant increase in $C_{16:0}$ and $C_{18:0}$ hepatic ceramide species and a corresponding lowering of hepatic sphingosine and sphingosine-1-phosphate species (Fig. 1b). In parallel, a significant increase of $C_{16:0}$ ceramide species was observed in adipose tissue, accompanied by lower adipose sphingoid levels (Fig. 1c). Compared with WT mice, iKO mice exhibited significantly increased blood glucose levels during an OGTT (Fig. 1d), indicating impaired systemic glucose tolerance. However, plasma

insulin levels during the OGTT were not different (Fig. 1e). There were no differences in glucose tolerance and insulin sensitivity between iKO and WT mice fed standard chow for 6 weeks followed by chow-dox for 2 weeks (ESM Fig. 1e,f).

To identify the specific tissues responsible for the deterioration in glucose homeostasis and insulin sensitivity, we performed hyperinsulinaemic–euglycaemic clamp studies in a cohort of iKO and WT animals. The glucose infusion rate needed to maintain euglycaemic conditions (~8.33 mmol/l) was decreased in iKO mice (Fig. 1f), demonstrating a decrease in whole body insulin sensitivity. Whole body glucose disposal was not altered (ESM Fig. 1g), suggesting minimal effects on muscle insulin action. In contrast, hepatic glucose production was suppressed less efficiently in iKO mice (Fig. 1g), reflecting increased hepatic insulin resistance in iKO mice.

Acute depletion of APN results in reduced serum TG clearance and decreased lipase activity

To assess the effects of the acute loss of APN on systemic lipid homeostasis, we performed a TGTT by gavaging a lipid emulsion (20% intralipid) in WT and iKO mice fed an HFD for 6 weeks followed by HFD-dox for 2 weeks. The HFD-fed iKO mice peaked at higher levels compared with WT mice demonstrating TG intolerance (Fig. 1h). Interestingly chow-fed iKO mice also had higher peaks of serum TG (ESM Fig. 1h). APN enhances capillary LPL activity to promote fatty acid translocation in tissues. Both pre- and post-heparin lipoprotein, hepatic and total lipase activity levels were measured in WT and iKO mice on chow-dox. In the pre-heparin state, iKO mice displayed reduced total and hepatic lipase activity (ESM Fig. 1i). In the post-heparin state, iKO mice displayed reduced total and LPL activity (ESM Fig. 1j). To further investigate the role of APN depletion in lipid metabolism, we intravenously injected a ^{3}H-triolein tracer into iKO and WT mice, enabling assessment of lipid uptake and β-oxidation rates in different tissues. iKO mice displayed increased hepatic lipid uptake with concurrent decreases in gonadal and mesenteric fat pads (Fig. 1i). Even though the changes in lipid oxidation did not significantly differ between iKO and WT mice (ESM Fig. 1k), isolation of mitochondria from iKO mice livers revealed significantly lower OCRs, reflecting a lower level of mitochondrial lipid oxidation (Fig. 1j).

FGF21 is capable of mobilising intracellular APN in iKO mice

Previous studies have shown that FGF21 increases adipocyte secretion of APN [20]. Furthermore, although APN has a relatively short half-life (<1 h) once in circulation, significant levels of APN are retained in the secretory pathway of adipocytes. To date, it is not clear whether this intracellular material reflects misfolded protein or whether it is 'secretion competent'. Interestingly, using the iKO mouse, we found that APN is still present in sWAT following complete depletion in serum (ESM Fig. 2a). The amount of APN in the subcutaneous depot after complete depletion in serum is ~25% of normal WT levels (ESM Fig. 2b).

We used FGF21 treatment to determine the secretion competency of the intracellular APN. Mice were fed chow-dox for 2 weeks and then treated with FGF21. An increase in circulating APN was detected 30 min after FGF21 treatment (Fig. 2a). However, this

increase in serum APN was transient, as APN levels were not detectable after 1 day. There was also a concomitant lowering of hepatic and adipose tissue levels of $C_{16:0}$ and $C_{18:0}$ ceramides (Fig. 2b,c). However, this decrease was not observed when congenital APNKO mice were treated with similar doses of FGF21 (ESM Fig. 2c,d).

Pioglitazone treatment leads to the generation of new APN-producing adipocytes in iKO mice

Thiazolidinediones (TZDs) are potent agonists for the key adipogenic transcription factor PPARγ. To investigate the effect of TZDs in iKO mice, we induced complete *Adipoq* deletion via chow-dox. Following cessation of doxycycline exposure, iKO and WT mice were fed an HFD supplemented with pioglitazone, a TZD known to improve insulin sensitivity by promoting adipogenesis. Any new cells that emerge as a result of TZD treatment will retain a functional copy of their *Adipoq* gene. After 28 days, APN re-emerged in serum, presumably as a result of the development of new adipocytes (Fig. 2d). APN levels gradually increased throughout 60 days of pioglitazone treatment. At 60 days, serum glucose levels in pioglitazone-treated iKO mice were significantly lower compared with untreated iKO mice; however, the levels were still higher than treated WT mice (Fig. 2e). Serum APN in iKO mice was reconstituted to ~50% of WT levels (ESM Fig. 2e). To confirm that APN was originating from new adipocytes, we performed an RNAscope analysis. We detected *Adipoq*-specific mRNA transcripts in the adipose tissue of WT mice, and confirmed that both iKO and WT mice treated with pioglitazone had *Adipoq* RNA transcripts in adipose tissue after 60 days (ESM Fig. 2f). APNKO mice given pioglitazone had no *Adipoq* RNA transcripts. These findings are consistent with the partial improvement seen in the iKO mice in response to TZD exposure. However, it is surprising that 50% of APN can be reconstituted with de novo adipogenesis within 60 days.

APN is critical for lipid metabolism in STZ-induced insulinopenic diabetes

To further elucidate the critical role of APN in lipid metabolism, we treated iKO, APNKO and WT mice with a high dose of STZ to effectively destroy beta cells. Serum glucose levels were elevated within 2 days in all groups treated with STZ (ESM Fig. 2g). After 4 days, iKO mice exhibited drastically less subcutaneous fat on CT imaging compared with both APNKO and WT mice (Fig. 2f). iKO mice had lower total body adipose tissue mass than WT and APNKO mice (Fig. 2g and ESM Fig. 2h). The more severe deterioration in lipid metabolism in iKO mice following STZ treatment was also apparent as a significant increase in circulating TG levels during a TGTT compared with both APNKO and WT mice (Fig. 2h). Consistent with the observations in the PANIC-ATTAC model, STZ-treated APNKO mice had a significantly lower survival rate than WT controls [21]. iKO mice showed an even more dramatic reduction in survival rate than APNKO mice (Fig. 2i). Following exposure to STZ, 30% of iKO mice died within 3 days and only 10% survived past 14 days compared with 50% of the APNKO mice.

Acute deletion of *Adipoq* induces an inflammatory gene signature in adipose tissue

To compare the gene signatures of adipose tissue in iKO and WT mice, sWAT was subjected to microarray analysis after 4 weeks of HFD followed by 2 weeks of HFD-dox. Principle component analysis was performed using all 45,000 probe sets across the two groups. The

genetic signature of the subcutaneous tissue was distinctly different between the iKO and WT mice (Fig. 3a). Heatmaps of the 150 most differentially expressed genes between iKO and WT were generated (Fig. 3b and ESM Table 3). The majority of these genes were significantly upregulated in the iKO group. Gene ontology analysis focused on genes that were significantly up or downregulated by at least 1.5-fold. Functional classification indicated that the most downregulated genes were related to insulin receptor activation (Fig. 3c and ESM Fig. 3a). Interestingly, the classifications of the most significantly upregulated genes were related to leucocyte and lymphocyte activation, and the regulation of the immune system (Fig. 3d and ESM Fig. 3b). These findings suggest that the insulin resistance resulting from acute APN depletion is triggered, at least in part, by immune activation. F4/80 immunohistochemistry staining confirmed that fat pads in iKO mice had increased levels of infiltrating macrophages and increased cellularity of sWAT compared with those of WT mice (Fig. 3e and ESM Fig. 3c). At the transcriptional level, major adipose tissue markers, such as *Adipsin*, *Lpl* and *Pparγ2*, were significantly decreased in iKO mouse sWAT; in addition to increases in immune cell activation markers *Lck*, *Lsp1* and *Cd6* (Fig. 3f). Previously we have shown that subcutaneous adipocytes develop during embryonic days 14–18, whereas other fat pads develop postnatally [12]. To study the loss of APN specifically in the subcutaneous adipose tissue, we used mice whose mothers received doxycycline from embryonic day 14 up to the time of delivery. One month after birth, serum APN was quantified in 'subcutaneous-specific knockouts' of *Adipoq* (sWAT-KO) mice. In sWAT-KO mice, serum APN levels were 66% and levels in subcutaneous tissue were 73% of WT mice (Fig. 3g and ESM Fig. 3d,e). Finally, the transcriptional signature of the sWAT in sWAT-KO mice was similar to that seen for iKO vs WT mice, but even more dramatic in terms of magnitude of the changes (Fig. 3h). Major adipose tissue markers, such as *Adipsin* and *Pparγ2*, were also strikingly lower in the sWAT-KO mice compared with WT mice.

Interestingly, although the liver is the major target organ of APN, we did not find any significant changes when we compared the gene signatures of iKO and WT livers 3 days after APN was depleted from serum (ESM Fig. 3f). From this, we can conclude that, although acute APN depletion results in immediate upregulation of inflammatory genes and downregulation of insulin signalling genes in adipose tissue, it takes a more prolonged absence of APN to incur transcriptional changes in the liver.

Discussion

Here we present the first model in which the acute depletion of APN can be induced in adult mice, thereby bypassing any compensatory mechanisms associated with constitutive, congenital loss-of-function mouse models and providing the opportunity to study the metabolic effects of acute deletion of *Adipoq* in adult mice. There are a number of limitations with the congenital models. First, APN is part of a larger superfamily of proteins that also comprise the CTRPs (C1q-TNF-α-related proteins), some of which are expressed in adipose tissue [22]. While no compensatory upregulation of any of these proteins has been reported, we cannot exclude the possibility that under some physiological conditions such compensatory upregulation may become relevant. Second, as reported for leptin, adipose-derived hormones may play an important developmental role in the formation of

hypothalamic circuits [23, 24]. A similar requirement for APN during development cannot be excluded.

With this novel mouse model, we demonstrate that the acute depletion of APN results in systemic insulin resistance and hyperlipidaemia, more severe in terms of its phenotypic manifestations than congenital loss of APN. Interestingly, the effects on systemic glucose homeostasis and insulin sensitivity are only observed if the mice are initially challenged with an HFD, while its effects on lipid homeostasis are independent of prior exposure to an HFD. These diet-dependent effects on insulin sensitivity could be mediated through the action of APN on its receptor and the ensuing ceramidase activity. Our studies have shown that ceramides, which are synthesised exclusively from saturated fats, are capable of inducing insulin resistance both at the cellular and systemic level [14, 25–27]. We observed a significant increase in both adipose and liver ceramide levels in our iKO model after HFD feeding. This is consistent with our recent observations that APN receptor overexpression in liver or adipose tissue triggers rapid reductions in tissue and plasma ceramide levels. These effects of the receptors are strictly dependent on the presence of APN [7]. Furthermore, recent structural insights into the APN receptors point directly at a receptor-inherent ceramidase activity and further highlights the sphingolipid axis as a major primary mediator of APN effects [28, 29].

Our model has also shown that, upon depletion of serum APN, a pool of intracellular APN is retained. This pool can be released into circulation by FGF21 and exerts ceramide-lowering effects in both liver and adipose tissue, indicating that this intracellular APN has potent bioactivity. Congenital APNKO mice lacking this pool of intracellular APN were not responsive to FGF21 treatment and the ceramide-lowering effects were not observed. These findings confirm previous observations that APN mediates the metabolic effects of FGF21 [20, 30]. A recent study by BonDurant et al challenges all the aforementioned studies [31]. The authors found that FGF21 did not have a significant effect on plasma APN levels and that APN was not required for the chronic effects of FGF21. Their findings are hard to explain considering evidence to the contrary from many different laboratories. One possible explanation lies in the unconventional APNKO mouse used by BonDurant et al for their studies. This model, by Ma et al [10], is the only APNKO mouse which fails to exhibit any phenotype of insulin resistance or hyperlipidaemia. Furthermore, the source and dosing of the recombinant FGF21 used may also contribute to the differences. Although our current study does not refute the observation that FGF21 may have APN-independent effects under some conditions, it does provide further evidence that APN is a mediator of FGF21 action.

Our findings also confirm our previous studies showing that APN is indispensable for survival in insulinopenic conditions. In Ye et al in 2014, we showed that when insulin levels decrease by >90%, due to widespread beta cell death, APNKO mice had a dramatically lower survival rate [21]. In our current study, the iKO mice had an even more dramatic reduction in survival rate. Under insulinopenic conditions, 30% of the iKO mice died in 3 days and only 10% survived past 14 days compared with 50% of the APNKO mice. Considering that iKO mice exhibit a more severe phenotype than the APNKO mice, these observations independently confirm the central role of APN in maintaining lipid homeostasis.

Microarray data from the iKO mice, compared with WT mice, show that the gene expression signatures of subcutaneous adipose tissues are distinctly unique. Interestingly, gene ontology analysis showed that the most upregulated groups of genes following acute *Adipoq* deletion were related to regulation of inflammation and leucocyte activation in subcutaneous tissue, which was confirmed through F4/80 staining that showed increased macrophage localisation in the fat pad of iKO mice. This suggests that a major role of APN in maintaining adipose tissue health is to suppress local inflammation. Furthermore, qPCR from sWAT of iKO mice showed dramatically lower levels of important adipogenic genes, such as *Pparγ2*, within 2 weeks of acute APN depletion. In summary, just days following acute APN depletion, the fat pad in iKO mice is highly inflammatory and dystrophic at a transcriptional level.

Collectively, our data show that acute depletion of APN results in a much more profound negative metabolic phenotype compared with constitutive models. Specifically, our data demonstrate that acute depletion of APN is especially detrimental to lipid homeostasis, under basal and particularly under insulinopenic conditions. Under insulinopenic conditions, the iKO mice had much lower survival rates compared with the congenital APN loss model. Furthermore, acute depletion of APN results in a highly proinflammatory gene signature in subcutaneous tissue. The phenotypic differences seen in acute vs chronic congenital loss of APN may give us a gradation of the severity of the effects and should systematically be pursued for other adipokines as well.

Supplementary Material

Refer to Web version on PubMed Central for supplementary material.

Acknowledgments

Abbreviations

|	
APN	Adiponectin
APNKO	Congenital adiponectin (*Adipoq*) knockout
APN-rtTA	*Adipoq* (APN) promoter-driven reverse tetracycline-controlled transactivator
Chow-dox	Chow diet supplemented with doxycycline
FGF21	Fibroblast growth factor 21
HFD	High-fat diet

HFD-dox	High-fat diet supplemented with doxycycline
iKO	Inducible *Adipoq* knockout
LPL	Lipoprotein lipase
OCR	Oxygen consumption rates
STZ	Streptozotocin
sWAT	Subcutaneous white adipose tissue
sWAT-KO	Subcutaneous white adipose tissue deletion of *Adipoq* TG, Triacylglycerol
TGTT	Triacylglycerol tolerance test
TRE-Cre	*Tet*-responsive
Cre TZD	Thiazolidinedione
UTSW	University of Texas Southwestern
WAT	White adipose tissue
WT	Wild-type

References

1. Turer AT, Scherer PE. Adiponectin: mechanistic insights and clinical implications. Diabetologia. 2012; 55:2319–2326. [PubMed: 22688349]

2. Pischon T, Hotamisligil GS, Rimm EB. Adiponectin: stability in plasma over 36 hours and within-person variation over 1 year. Clin Chem. 2003; 49:650–652. [PubMed: 12651819]

3. Hotta K, Funahashi T, Bodkin NL, et al. Circulating concentrations of the adipocyte protein adiponectin are decreased in parallel with reduced insulin sensitivity during the progression to type 2 diabetes in rhesus monkeys. Diabetes. 2001; 50:1126–1133. [PubMed: 11334417]

4. Berg AH, Combs TP, Scherer PE. ACRP30/adiponectin: an adipokine regulating glucose and lipid metabolism. Trends Endocrinol Metab. 2002; 13:84–89. [PubMed: 11854024]

5. Combs TP, Berg AH, Obici S, Scherer PE, Rossetti L. Endogenous glucose production is inhibited by the adipose-derived protein Acrp30. J Clin Invest. 2001; 108:1875–1881. [PubMed: 11748271]

6. Combs TP, Pajvani UB, Berg AH, et al. A transgenic mouse with a deletion in the collagenous domain of adiponectin displays elevated circulating adiponectin and improved insulin sensitivity. Endocrinology. 2004; 145:367–383. [PubMed: 14576179]

7. Holland WL, Xia JY, Johnson JA, et al. Inducible overexpression of adiponectin receptors highlight the roles of adiponectin-induced ceramidase signaling in lipid and glucose homeostasis. Mol Metab. 2017; 6:267–275. [PubMed: 28271033]

8. Kubota N, Terauchi Y, Yamauchi T, et al. Disruption of adiponectin causes insulin resistance and neointimal formation. J Biol Chem. 2002; 277:25863–25866. [PubMed: 12032136]

9. Maeda N, Shimomura I, Kishida K, et al. Diet-induced insulin resistance in mice lacking adiponectin/ACRP30. Nat Med. 2002; 8:731–737. [PubMed: 12068289]

10. Ma K, Cabrero A, Saha PK, et al. Increased beta -oxidation but no insulin resistance or glucose intolerance in mice lacking adiponectin. J Biol Chem. 2002; 277:34658–34661. [PubMed: 12151381]

11. Nawrocki AR, Rajala MW, Tomas E, et al. Mice lacking adiponectin show decreased hepatic insulin sensitivity and reduced responsiveness to peroxisome proliferator-activated receptor gamma agonists. J Biol Chem. 2006; 281:2654–2660. [PubMed: 16326714]

12. Wang QA, Tao C, Gupta RK, Scherer PE. Tracking adipogenesis during white adipose tissue development, expansion and regeneration. Nat Med. 2013; 19:1338–1344. [PubMed: 23995282]

13. Schraw T, Wang ZV, Halberg N, Hawkins M, Scherer PE. Plasma adiponectin complexes have distinct biochemical characteristics. Endocrinology. 2008; 149:2270–2282. [PubMed: 18202126]

14. Holland WL, Miller RA, Wang ZV, et al. Receptor-mediated activation of ceramidase activity initiates the pleiotropic actions of adiponectin. Nat Med. 2011; 17:55–63. [PubMed: 21186369]

15. Kusminski CM, Holland WL, Sun K, et al. MitoNEET-driven alterations in adipocyte mitochondrial activity reveal a crucial adaptive process that preserves insulin sensitivity in obesity. Nat Med. 2012; 18:1539–1549. [PubMed: 22961109]

16. Livak KJ, Schmittgen TD. Analysis of relative gene expression data using real-time quantitative PCR and the $2^{-\Delta\Delta Ct}$ Method. Methods. 2001; 25:402–408. [PubMed: 11846609]

17. Asterholm IW, Scherer PE. Enhanced metabolic flexibility associated with elevated adiponectin levels. Am J Pathol. 2010; 176:1364–1376. [PubMed: 20093494]

18. Xu Y, Wu Z, Sun H, et al. Glutamate mediates the function of melanocortin receptor 4 on Sim1 neurons in body weight regulation. Cell Metab. 2013; 18:860–870. [PubMed: 24315371]

19. Razani B, Combs TP, Wang XB, et al. Caveolin-1-deficient mice are lean, resistant to diet-induced obesity, and show hypertriglyceridemia with adipocyte abnormalities. J Biol Chem. 2002; 277:8635–8647. [PubMed: 11739396]

20. Holland WL, Adams AC, Brozinick JT, et al. An FGF21-adiponectin-ceramide axis controls energy expenditure and insulin action in mice. Cell Metab. 2013; 17:790–797. [PubMed: 23663742]

21. Ye R, Holland WL, Gordillo R, et al. Adiponectin is essential for lipid homeostasis and survival under insulin deficiency and promotes beta-cell regeneration. Elife. 2014; :3.doi: 10.7554/eLife. 03851

22. Davis KE, Scherer PE. Adiponectin: no longer the lone soul in the fight against insulin resistance? Biochem J. 2008; 416:e7–e9. [PubMed: 18990088]

23. Bouret SG, Bates SH, Chen S, Myers MG Jr, Simerly RB. Distinct roles for specific leptin receptor signals in the development of hypothalamic feeding circuits. J Neurosci. 2012; 32:1244–1252. [PubMed: 22279209]

24. Bouret SG, Draper SJ, Simerly RB. Trophic action of leptin on hypothalamic neurons that regulate feeding. Science. 2004; 304:108–110. [PubMed: 15064420]

25. Xia JY, Holland WL, Kusminski CM, et al. Targeted induction of ceramide degradation leads to improved systemic metabolism and reduced hepatic steatosis. Cell Metab. 2015; 22:266–278. [PubMed: 26190650]

26. Holland WL, Brozinick JT, Wang LP, et al. Inhibition of ceramide synthesis ameliorates glucocorticoid-, saturated-fat-, and obesity-induced insulin resistance. Cell Metab. 2007; 5:167–179. [PubMed: 17339025]

27. Turpin SM, Nicholls HT, Willmes DM, et al. Obesity-induced CerS6-dependent C16:0 ceramide production promotes weight gain and glucose intolerance. Cell Metab. 2014; 20:678–686. [PubMed: 25295788]

28. Holland WL, Scherer PE. Structural biology: receptors grease the metabolic wheels. Nature. 2017; 544:42–44. [PubMed: 28329767]

29. Vasiliauskaite-Brooks I, Sounier R, Rochaix P, et al. Structural insights into adiponectin receptors suggest ceramidase activity. Nature. 2017; 544:120–123. [PubMed: 28329765]

30. Lin Z, Tian H, Lam KS, et al. Adiponectin mediates the metabolic effects of FGF21 on glucose homeostasis and insulin sensitivity in mice. Cell Metab. 2013; 17:779–789. [PubMed: 23663741]

31. BonDurant LD, Ameka M, Naber MC, et al. FGF21 Regulates Metabolism Through Adipose-Dependent and -Independent Mechanisms. Cell Metab. 2017; 25:935–944e4. [PubMed: 28380381]
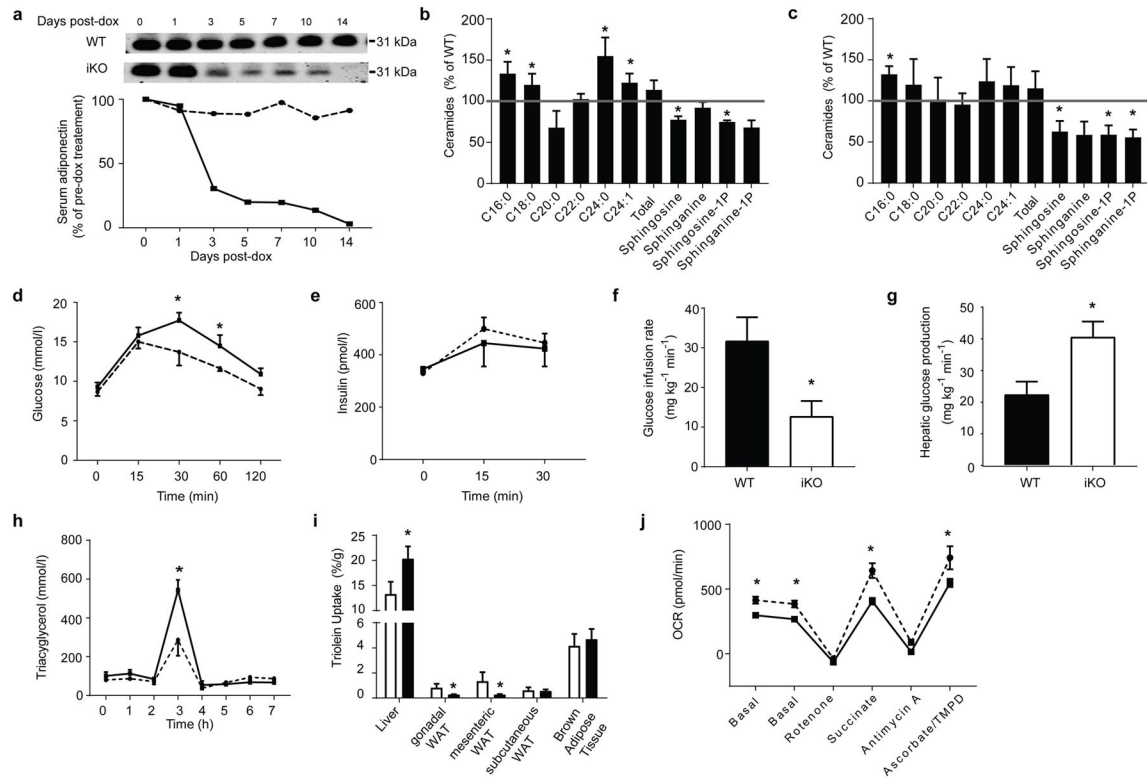
Fig. 1.

Inducible adipose-specific deletion of *Adipoq* results in significantly elevated $C_{16:0}$ ceramide species in liver and adipose tissue, and worsened total body glucose and lipid homeostasis in HFD-fed mice. (**a**) Representative immunoblots of serum APN of iKO mice (solid line) and WT (dashed line) littermate controls; dox, doxycycline. (**b**) Analysis of liver ceramide and sphingoid species from iKO (*n*=8) mice and WT (*n*=8) littermates. (**c**) Analysis of subcutaneous adipose tissue ceramide and sphingoid species from iKO (*n*=8) mice and WT (*n*=8) littermates. (**d**) Circulating glucose levels measured during an OGTT for iKO (solid line, *n*=6) and WT (dashed line, *n*=7) mice (2.5 g/kg glucose per oral gavage). (**e**) Serum insulin levels during the OGTT were quantified via ELISA for iKO (solid line) and WT (dashed line) mice. (**f**) Glucose infusion rates during hyperinsulinaemic–euglycaemic clamp experiments performed on conscious, unrestrained WT (*n*=6) and iKO (*n*=6) mice. (**g**) Hepatic glucose output during hyperinsulinaemic euglycaemic clamp experiments performed on conscious, unrestrained WT (*n*=6) and iKO (*n*=6) mice. (**h**) Circulating TG levels were measured during an oral TGTT (20% intralipid, 15 μl/g; single gavage) in iKO (solid line, *n*=8) mice and WT (dashed line, *n*=8) littermate controls. In (**a**–**h**), mice were fed an HFD for 6 weeks then HFD-dox for 2 weeks. (**i**) Total ^{3}H-triolein lipid uptake per tissue 15 min after injection (74000 Bq per mouse in 100 μl of 5% intralipid, single tail vein injection) in male iKO (black bars, *n*=6) and WT (white bars, *n*=6) mice fed HFD-dox for 4 weeks; gWAT, gonadal WAT; mWAT, mesenteric WAT; BAT, brown adipose tissue. (**j**) OCRs in isolated mitochondria (5 μg mitochondrial protein per well) derived from liver tissue of iKO (solid line, *n*=3) vs WT (dashed line, *n*=3) mice fed HFD-dox for 4 weeks. Basal conditions contained the substrates pyruvate and malate; subsequent substrates included

succinate and ascorbate. Serum depletion of APN was confirmed with immunoblotting prior to the initiation of all metabolic studies. *$p < 0.05$ vs WT, by Student's *t* test
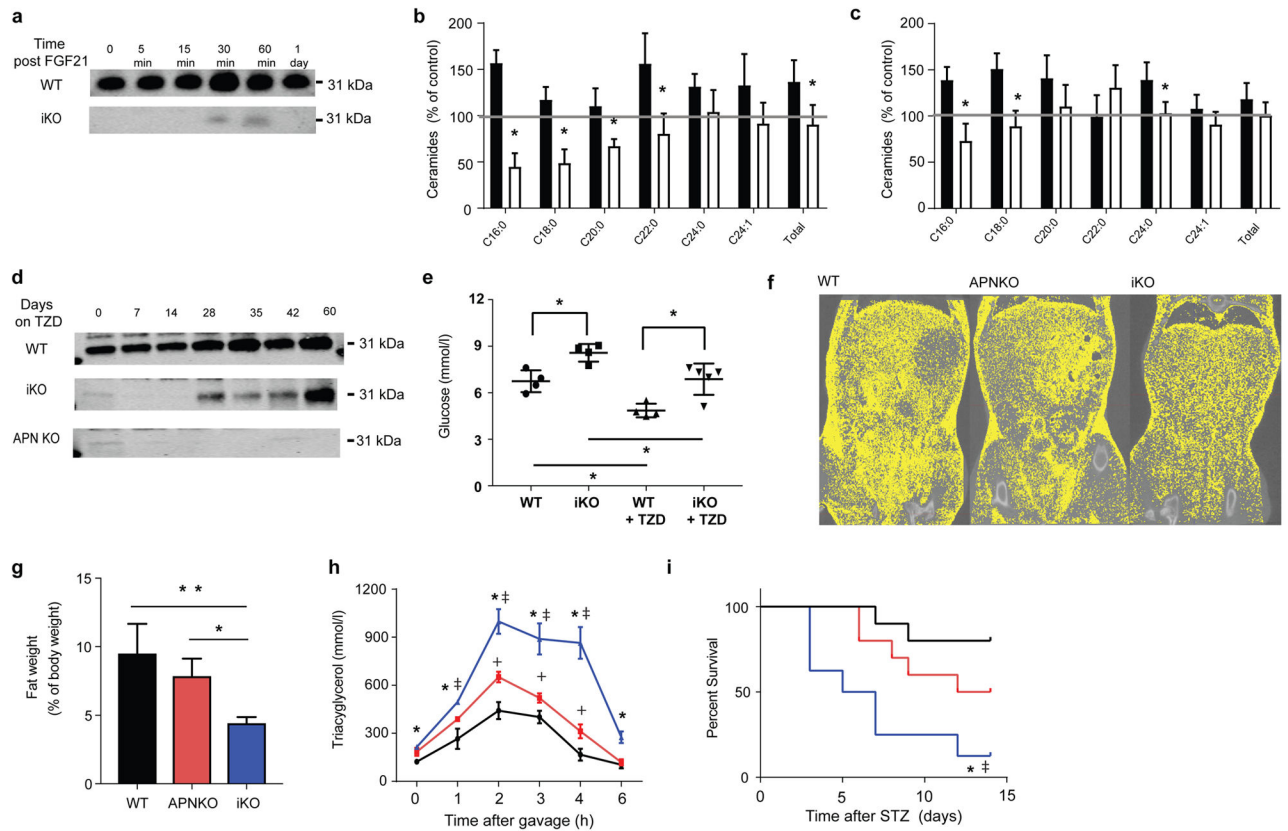
Fig. 2.

FGF21 and TZDs are capable of increasing serum APN levels in APN$^{fl/fl}$ mice fed chow-dox for 2 weeks. (**a**) Representative immunoblot of serum APN levels 1 day post intraperitoneal injection of FGF21 (2 mg/kg) in iKO and WT mice. (**b**) Analysis of liver ceramide species 1 day after intraperitoneal injection of FGF21 (2 mg/kg) in iKO mice, treated (white bars, n=7) and untreated (black bars, n=7). (**c**) Analysis of sWAT ceramide species 1 day after intraperitoneal injection of FGF21 (2 mg/kg) in iKO mice, treated (white bars, n=7) and untreated (black bars, n=7). (**d**) Representative immunoblot of serum APN levels in iKO (n=5), WT (n=7), and APNKO (n=5) mice after 60 days of HFD containing pioglitazone (40 mg/kg). (**e**) Fasting glucose levels after 60 days of HFD or HFD containing pioglitazone (40 mg/kg) in iKO (n=5) and WT (n=7) mice. (**f**) Representative CT images 4 days post STZ injection in APNKO, iKO and WT mice. (**g**) Body fat weight, normalised to total body weight, 4 days post STZ injection for APNKO (n=8), iKO (n=6) and WT (n=8) mice. (**h**) Circulating TG levels measured during an oral TGTT (20% intralipid, 15 μl/g; single gavage) 4 days post STZ injection in APNKO (red line, n=8), iKO (blue line, n=6) and WT (black line, n=8) mice. (**i**) Post STZ injection survival curve for iKO (blue line, n=10), APNKO (red line, n=12) and WT (black line, n=10) mice given an intraperitoneal injection of STZ (150 μg/g). All mice were fed chow-dox for 2 weeks prior to tests. Serum depletion of APN was confirmed with immunoblotting prior to the initiation of all studies. In (**b, c**) *p<0.05 vs WT. In (**e, g**) *p<0.05, **p<0.01, as shown. In (**h**) $^{†}p$<0.05 for APNKO vs

WT; *$p<0.05$ for iKO vs WT; [‡]$p<0.05$ for iKO vs APNKO. In (**i**) *$p<0.05$ for iKO vs WT; [‡]$p<0.05$ for APNKO vs WT
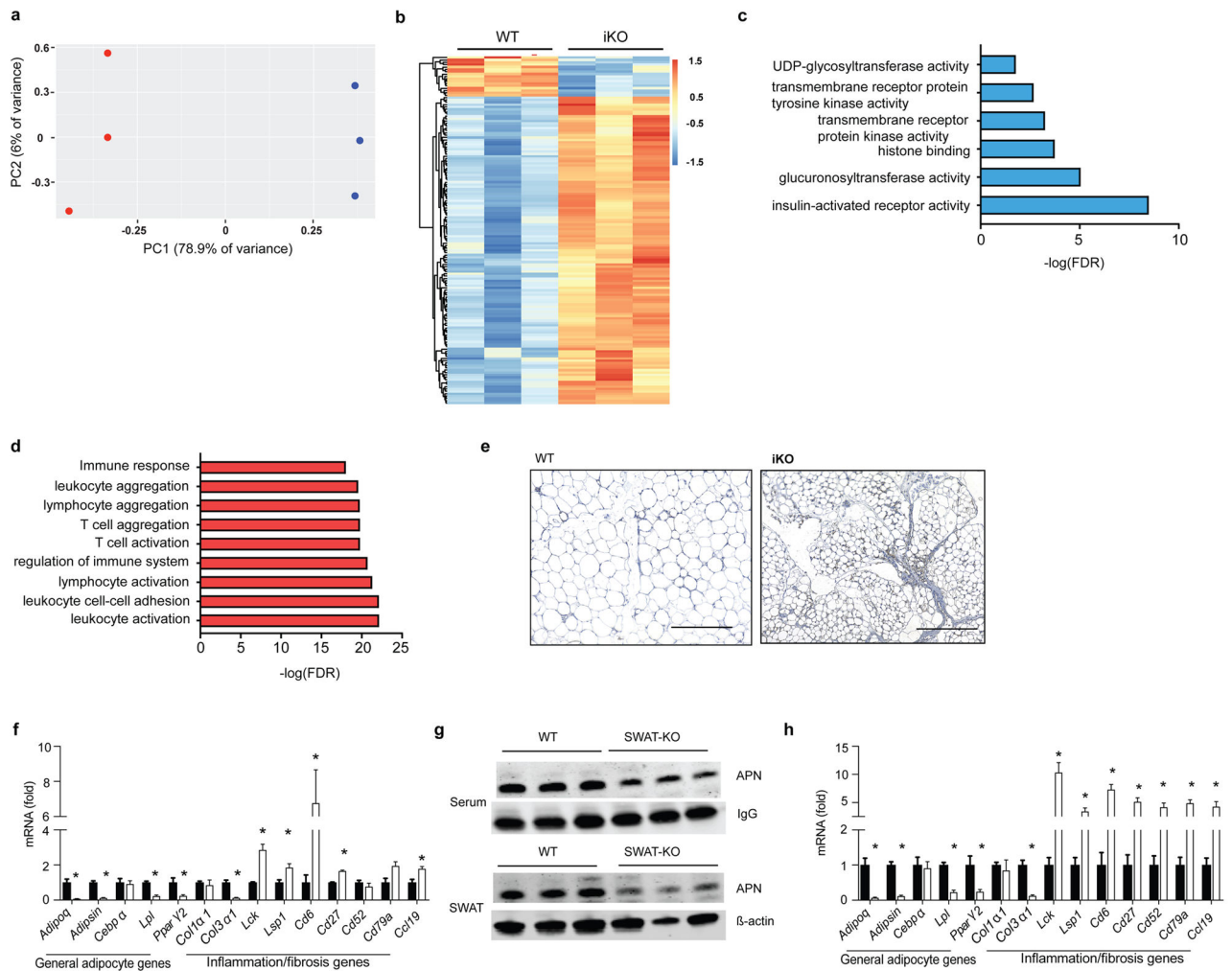
Fig. 3.
Microarray of sWAT after adipose-specific deletion of *Adipoq* in iKO and WT mice shows significant upregulation of inflammatory genes in iKO mice. (**a**) Principal component (PC) analysis performed on the significantly changed sWAT genes of iKO (blue dots, *n*=3) and WT (red dots, *n*=3) mice. (**b**) Heatmap of significantly upregulated and downregulated genes in sWAT of iKO and WT mice. (**c**) Gene ontology analysis (GOTERM_BP_FAT) of statistically significant downregulated sWAT genes of iKO mice with at least twofold change over WT mice, derived from (**b**). (**d**) Gene ontology analysis (GOTERM_MF_FAT) of statistically significant upregulated sWAT genes of iKO mice with at least twofold change over WT controls, derived from (**b**); FDR, false discovery rate. (**e**) Representative F4/80 immunohistochemistry of WT and iKO sWAT (scale bars, 400 μm). (**f**) mRNA levels of general adipocyte genes and inflammatory genes quantified using qPCR (normalised to *Rps18*) in whole subcutaneous adipose tissue of iKO (white bar, *n*=4) and WT (black bar, *n*=4) mice. In (**a**–**f**), iKO and WT mice were fed HFD for 4 weeks followed by 2 weeks of HFD-dox. (**g**) Representative immunoblots of serum and sWAT APN levels in WT (*n*=3) and sWAT-KO (*n*=3) mice at 1 month of age. (**h**) mRNA levels of general adipocyte genes and inflammatory genes quantified using qPCR (normalised to *Rps18*) in whole subcutaneous

adipose tissue of sWAT-KO (white bar, n=5) and WT (black bar, n=4) mice at 1 month of age. Serum depletion of APN was confirmed with immunoblotting prior to the initiation of all studies. *p<0.05 vs WT, by Student's t test